Journal of Structural Geology, Vol. 3, No. 2, pp. 117 to 128, 1981
Printed in Great Britain

0191-8141/81/020117-12 $02.00/0

Boudinage structure: some new interpretations based on elastic–plastic finite element simulations

G. E. LLOYD

Centre for Materials Science, University of Birmingham, Birmingham B15 2TT, U.K.

C. C. FERGUSON

Department of Geology, University of Nottingham, Nottingham NG7 2RD, U.K.

(*Received* 8 *September* 1980; *accepted in revised form* 5 *January* 1981)

Abstract—An elastic–plastic finite element method, based on the Prandtl–Reuss equations of plastic flow and involving equivalent stresses and strains, is used to study boudinage structure. Our choice of data for the simulations was guided by published stress–strain curves for marble (matrix) and quartzite (boudin), the essential parameters being yield stress and rock 'hardness' (defined by the slope of the stress–strain curve). All models assume an initial fracture and slight separation and therefore only simulate post-fracture behaviour. The simulations suggest that boudin shape is determined by boudin hardness; maximum stresses are concentrated in the corners which therefore shows the most shape modification. Matrix hardness determines the amount of boudin separation. Direct comparison with natural examples is restricted to boudins suffering no significant pre-fracture plastic deformation (i.e. rectangular- and barrel-shaped boudins), although other types are likely to have the characteristics of barrel and pinch-and-swell styles. The simulations do not consider the nature and timing of boudin-defining fractures but these are important in determining the style of boudinage which ultimately develops. Some mechanical problems associated with the infilling of inter-boudin gaps by ductile rock matrix are discussed and two models proposed. The first, based on yielding fracture mechanics, is used to explain boudins with wedge-shaped (or otherwise non-matching) ends. The second, a hydraulic model, is proposed to account for gaps between rectangular boudins that are filled by ductile rock matrix.

INTRODUCTION

THERE appear to have been only five contributions in the literature on the finite element simulation of boudinage structure. Four of these report the same work (Stephansson & Berner 1971, Stephansson 1973, Huddleston & Stephansson 1973, Stromgard 1973), which assumed elastic plane stress conditions and employed constant strain quadrilateral elements (although nodal displacements, stresses and strains were determined by breaking down the quadrilaterals into three-node triangular elements). Such triangular elements are computationally inefficient and may lead to relatively large numerical errors (Desai & Abel 1972). In addition, plane stress assumes that the structure being represented is a thin shell rather than a solid body of considerable thickness. A more realistic approach is to assume plane strain conditions. In spite of these drawbacks this early study did manage to explain some of the features of boudinage structure.

Recently, Selkman (1978) reported a more rigorous finite element study of the stress distribution and displacements during progressive boudinage, again assuming elastic behaviour. Although he used an iterative approach with a constant amount of shortening per deformation increment the shape modification and separation of the boudins were identical to those obtained by the earlier study and also by the present authors in an elastic plane strain analysis using isoparametric quadrilateral elements (in which the the strain need not be homogenous across the element). Because the plane strain and iterative approaches failed to produce significant improvements on the earlier simpler model further progress is likely to require the modelling of more realistic material behaviour. So far only linear elastic behaviour has been considered.

In this contribution we report the finite element simulation of boudinage structure in which plastic material behaviour is allowed. This requires the incorporation of constitutive equations of material plasticity into a standard finite element program. A simplified theory of plasticity is presented which is then adapted for use in finite element analysis. A series of simulations is then performed to study the effects of material properties and amount of deformation on the characteristic features of

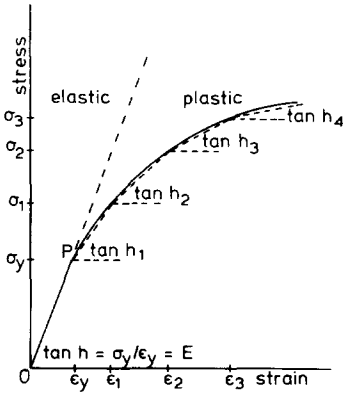

Fig. 1. Idealised stress–strain curve approximated by straight-line segments for use in the PFEM models.

boudinage, such as boudin shape and separation. The results of these simulations are then compared with natural examples of boudinage.

SIMPLIFIED PLASTICITY THEORY

Figure 1 shows an idealised stress–strain curve. At any point on the curve the stress–strain relationship can be written

$$\tan h = \frac{d\sigma}{d\varepsilon} \tag{1}$$

where h, the work-hardening coefficient, determines how the deformation can continue. Obviously the segment OP represents linear material behaviour, but for stresses above that at P, other types of material response are possible depending on whether the relative resistance to deformation increases or decreases. Equation (1) therefore reflects the internal response of the material to the deformation and all its possible forms can be represented phenomenologically by plasticity theory.

A material behaves in an elastic–plastic manner if, at stresses below a critical level, it responds as an elastic solid while at stresses at or above the critical level (yield stress) it becomes permanently strained. Mathematical theories of plastic deformation (e.g. Hill 1950, Mendelson 1968) express the stress history of a material as a line joining points of successive stress states, one of which is the yield stress. A variety of stress paths are usually possible and consequently a yield surface containing all the possible yield points can be envisaged. The shape of this surface is a function of the three invariants of the stress tensor and is known as the yield criterion. Von Mises has proposed the most generally accepted yield criterion which involves only the second invariant of the deviatoric stress tensor (see Ramsay 1967, p. 316).

In any constitutive equation for plastic behaviour the principal axes of the strain increments are parallel to those of the stress, and the incremental strains are proportional to the ratios of the stress magnitudes. Thus, the basic equations of plastic flow (Prandtl–Reuss equations) are (Ramsay 1967, p. 321):

$$\delta\varepsilon_{ii} = \frac{2}{3}\delta\psi\left[\sigma_{ii} - \frac{1}{2}(\sigma_{jj} + \sigma_{kk})\right] + \frac{1}{E}[\delta\sigma_{ii} - \nu(\delta\sigma_{ij} + \delta\sigma_{kk})]$$

$$\delta\varepsilon_{ij} = 2\delta\psi\sigma_{ij} + 2\frac{(1+\nu)}{E}\sigma_{ij} \tag{2}$$

where $\{i, j, k\}$ represent $\{x, y, z\}$ permutated in the usual way, E is Young's modulus and ν is Poisson's ratio; and ψ is a proportionality factor which relates strain increments to deviatoric stresses and which is independent of the yield criterion.

PLASTIC FINITE ELEMENT THEORY

The finite element method (FEM) is a numerical procedure for modelling forces, displacements (or velocities), stresses and strains (or strain-rates) in bodies of arbitrary geometry and for materials obeying a variety of constitutive equations. The continuous body is represented by a finite number of discrete elements connected at nodal points; material properties may vary from element to element. In most finite element simulations a relationship is required between the co-existing forces and displacements and leads to a definition of the stiffness of the body (Desai & Abel 1972),

$$[S] = \{F\}\{U\}^{-1} \tag{3}$$

where $[S]$ is the combined stiffness of all the elements in the body, $\{F\}$ the externally applied forces (or displacements) and $\{U\}$ the unknown displacements. This is the usual assumption of linearity and, if both $[S]$ and $\{F\}$ are known, leads to a simple evaluation of $\{U\}$. However, if either $[S]$ or $\{F\}$ or both are dependent on $\{U\}$ the relationship is nonlinear. So far most applications of the FEM in structural geology have considered either linear elastic or Newtonian viscous behaviour (e.g. Stephansson & Berner 1971, Shimamoto & Hara 1976) or nonlinear steady-state behaviour based on a power law creep expression (e.g. Parrish *et al.* 1976). To model nonlinear stress–strain relationships by means of plasticity theory requires a different technique based on the general theory outlined above.

In the elastic–plastic finite element method (PFEM) the uniaxial stress–strain curve is approximated by straight line segments, the first of which represents the elastic portion of the curve with gradient equal to Young's modulus. The plastic component is made up of much shorter linear segments with gradients equal to the strain-hardening coefficients. The uniaxial case is generalised by making use of equivalent stress (σ_{eq}) and equivalent strain (ε_{eq}). The equivalent stress is given by (Mendelson 1968).

$$\sigma_{eq} = \frac{1}{\sqrt{2}}[(\sigma_{xx} - \sigma_{yy})^2 + (\sigma_{yy} - \sigma_{zz})^2 + (\sigma_{zz} - \sigma_{xx})^2 + 6(\sigma_{xy}^2 + \sigma_{yz}^2 + \sigma_{zx}^2)] \tag{4a}$$

For the uniaxial case σ_{eq} is identical to σ_1, the maximum principal stress at a point (Mendelson 1968).

For ε_{eq} it is convenient, after yield has occurred, to partition the components of strain into elastic and plastic parts. The elastic components are related to the stresses through Hooke's law. The plastic components contribute nothing towards the stresses and form residual strains; they are zero before yield. The equivalent strain is therefore given by:

$$\varepsilon_{eq} = (\varepsilon_{eq})_{el} + (\varepsilon_{eq})_{pl} \tag{4b}$$

where the elastic component is,

$$(\varepsilon_{eq})_{el} = \frac{\sigma_{eq}}{E}$$

$$= \frac{1}{(1+\nu)\sqrt{2}}\{[(\varepsilon_{xx})_{el} - (\varepsilon_{yy})_{el}]^2 + [(\varepsilon_{yy})_{el} - (\varepsilon_{zz})_{el}]^2 + [(\varepsilon_{zz})_{el} - (\varepsilon_{xx})_{el}]^2 + \frac{3}{2}[(\varepsilon_{xy})_{el}^2 + (\varepsilon_{yz})_{el}^2 + (\varepsilon_{zx})_{el}^2]\}^{1/2} \quad (5a)$$

and the plastic component is given by the sum of the increments of the equivalent plastic strains (Mendelson 1968),

$$(\delta\varepsilon_{eq})_{pl} = \frac{2}{3\sqrt{2}}\{[(\delta\varepsilon_{xx})_{pl} - (\delta\varepsilon_{yy})_{pl}]^2 + [(\delta\varepsilon_{yy})_{pl} - (\delta\varepsilon)_{zz}]^2 + [(\delta\varepsilon_{zz})_{pl} - (\delta\varepsilon_{xx})_{pl}]^2 + \frac{3}{2}[(\delta\varepsilon_{xy})_{pl}^2 + (\delta\varepsilon_{yz})_{pl}^2 + (\delta\varepsilon_{zx})_{pl}^2]\}^{1/2}. \quad (5b)$$

Here, making the usual assumption of no volume change, $\frac{3}{2}$ replaces $(1 + \nu)$ and $(\delta\varepsilon_{xx})_{pl} + (\delta\varepsilon_{yy})_{pl} + (\delta\varepsilon_{zz})_{pl} = 0$. The constants in equations (4a), (5a) and (5b) are chosen so that σ_{eq} and ε_{eq} for the uniaxial case are simply σ_{xx} and ε_{xx}. When σ_{eq} becomes greater than the uniaxial yield stress yielding occurs according to the von Mises criterion.

The expression for $(\varepsilon_{eq})_{pl}$ is similar to that for σ_{eq} and complies with the plastic stress–strain relationships and the principle of the equivalence of plastic work, which states that the deformation is a function of the plastic work only and must be positive or zero (Mendelson 1968). The equivalent strain must therefore be expressed as the sum of its increments (i.e. $(\delta\varepsilon_{xx})_{pl}$ etc.). We are now in a position to define the elastic–plastic stress–strain relations.

The elastic part of the strain components are related to the stresses by Hooke's law. For the plastic stress–strain relations the PFEM uses the Prandtl–Reuss equations (2). However, because we have already accounted for the elastic part of the total deformation we are only concerned with the plastic terms in equations (2) which can be written,

$$(\delta\varepsilon_{xx})_{pl} = \delta\psi\left[\sigma_{xx} - \frac{1}{3}(\sigma_{xx} + \sigma_{yy} + \sigma_{zz})\right] \text{etc.}$$

in which $\frac{1}{3}(\sigma_{xx} + \sigma_{yy} + \sigma_{zz})$ is the mean stress. Thus,

$$(\delta\varepsilon_{xx})_{pl} = \delta\psi\sigma'_{xx} \text{ etc.} \quad (6)$$

where σ'_{xx} is the deviatoric stress. We can now write the total elastic–plastic stress–strain relationships by making the appropriate substitutions into equations (2). Hence,

$$\delta\varepsilon_{xx} = \delta\psi\sigma'_{xx} + \frac{1}{E}[\sigma_{xx} - \nu(\sigma_{yy} + \sigma_{zz})] \text{ etc.}$$

Using the definitions of σ_{eq} and $(\delta\varepsilon_{eq})_{pl}$ given by equations (4a) and (5b) we can also define,

$$\delta\psi = \frac{3}{2}\frac{(\delta\varepsilon_{eq})_{pl}}{\sigma_{eq}}.$$

The constitutive equation used in the PFEM can now be written

$$\delta\varepsilon_{xx} = \frac{3}{2}\frac{(\delta\varepsilon_{eq})_{pl}}{\sigma_{eq}}\sigma'_{xx} + \frac{1}{E}[\sigma_{xx} - \nu(\sigma_{yy} + \sigma_{zz})] \text{ etc.}$$

$$\delta\varepsilon_{xy} = \frac{3}{2}\frac{(\delta\varepsilon_{eq})_{pl}}{\sigma_{eq}}\sigma_{xy} + \frac{2(1+\nu)}{E}\sigma_{xy} \text{ etc.} \quad (7)$$

As the plasticity analysis is based on the incremental Prandtl–Reuss equations it is normally necessary to apply the total load over the structure in load increments. When the first load increment is applied, the strains, and therefore the stresses, are calculated for each element at particular points. Where yielding has occurred the stresses are given an equivalent stress value greater than the yield stress. To begin with, the plastic strains are taken as zero and so the equivalent stress and the equivalent strain will lie on the continuation of the linear (elastic) part of the stress–strain curve (Fig. 1) and not on the curve itself. A negative gradient is therefore taken from the calculated point onto the true curve so as to estimate the value of the equivalent plastic strain increment. Then, given the equivalent stress and the equivalent strain, the PFEM checks to see whether the point fits onto the actual curve. If it does, the analysis proceeds to the next load increment and the process is repeated; if it does not, the program uses the equivalent stress and strain to make a new estimate of the equivalent plastic strain from the curve, calculates a new value for the plastic strain increments and repeats the fitting. The process continues until the calculated point lies on the actual curve. The final values are then used to calculate the displacements and forces within the body.

To model plastic deformation using the PFEM, we require data on the yield stresses, the (strain-hardening) gradients of the linear segments of the plastic parts of the stress–strain curve, the value of the stresses at the intersection of adjacent segments and the elastic constants of the pre-plastic deformation. The acquisition of this data is discussed in the next section.

MODEL CONFIGURATION AND ASSUMPTIONS

The general forms of stress–strain curves derived from experimental deformations of rocks are shown in Fig. 2(a). In the PFEM simulations our choice of values for yield stress and strain-hardening gradient has been guided by the experimental curves for Yule marble extended parallel to foliation (Heard & Raleigh 1972) and 'dry' quartzite (Heard & Carter 1968, but taken from Parrish *et al.* 1976). The experimental conditions were 700°C and a strain rate of 10^{-7} s^{-1}. Geologically this is very fast, but the high temperature is considered to produce deformation by mechanisms similar to those operating in nature at slower strain-rates and lower temperatures (Paterson 1976).

The yield stress is defined by the point on the curve (Fig. 2a) below which the stress–strain relationship is linear. Above the yield stress the curve is divided into linear segments h_1, h_2, etc. To describe the curve above yield stress the PFEM requires the value of h_1, h_2, etc. and the magnitude of the stress (σ_1, σ_2, etc.) at the intersection of

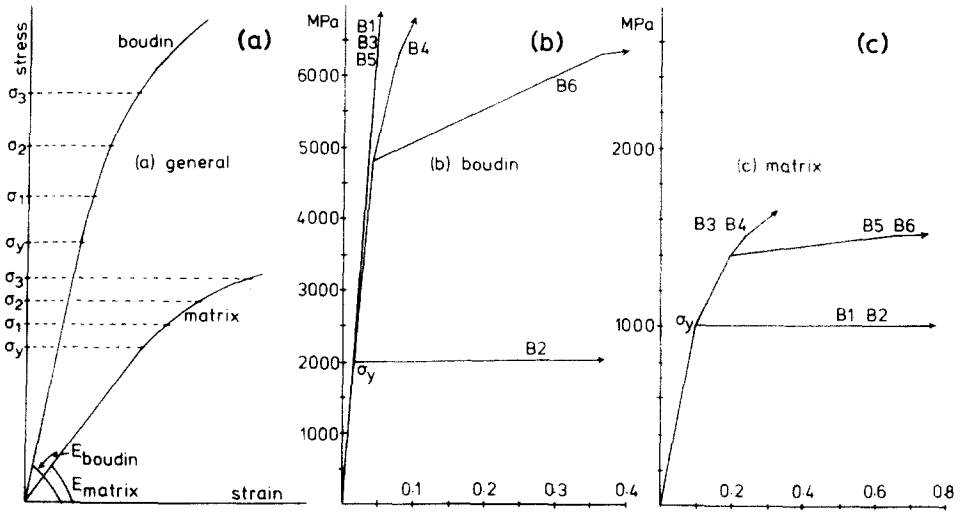

Fig. 2. (a) Generalised stress–strain curves for boudin and matrix used in the FEM models showing how the data were obtained. (b) Stress–strain curves for the boudins, modified from experimental deformation data given by Heard & Carter (1968). (c) Stress–strain curves for the matrix, modified from experimental deformation data given by Heard & Raleigh (1972).

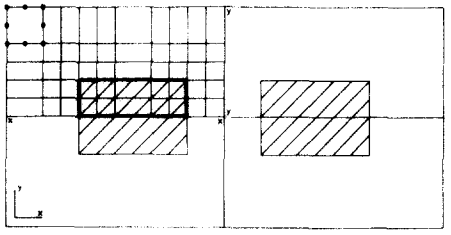

Fig. 3. Model configuration; because of symmetry only one quarter of the whole system is required provided that the elemental nodes along *yy* and *xx* are constrained to move parallel to *y* and *x* respectively. Nodal positions are shown for one element, while the boudin elements are shaded.

the segments. The experimentally motivated curves used to represent various boudin–matrix relationships are shown in Figs. 2(b) and (c). In three simulations (B1, B3 and B5) only elastic deformation of the boudins is permitted. In the other models (B2, B4 and B6) plastic boudin deformation is allowed, the deformation history being controlled by the yield stress (the same for each model) and the value of the work-hardening coefficient for each deformation increment. In one model (B2) the boudin becomes perfectly plastic at a stress only slightly above the yield stress and we refer to this as a soft boudin. In the other two (B4 and B6) the work-hardening coefficient reduces very much less rapidly and is the same for both boudins until the final stages of deformation when B6 becomes softer; the boudins do not approach perfect plasticity and we refer to these as hard boudins, although B4 is ultimately harder than B6. The matrix, which can deform plastically in all models, is perfectly plastic (i.e. soft) in models B1 and B2 and (relatively) hard in models B3, B4, B5 and B6, although for the final stages

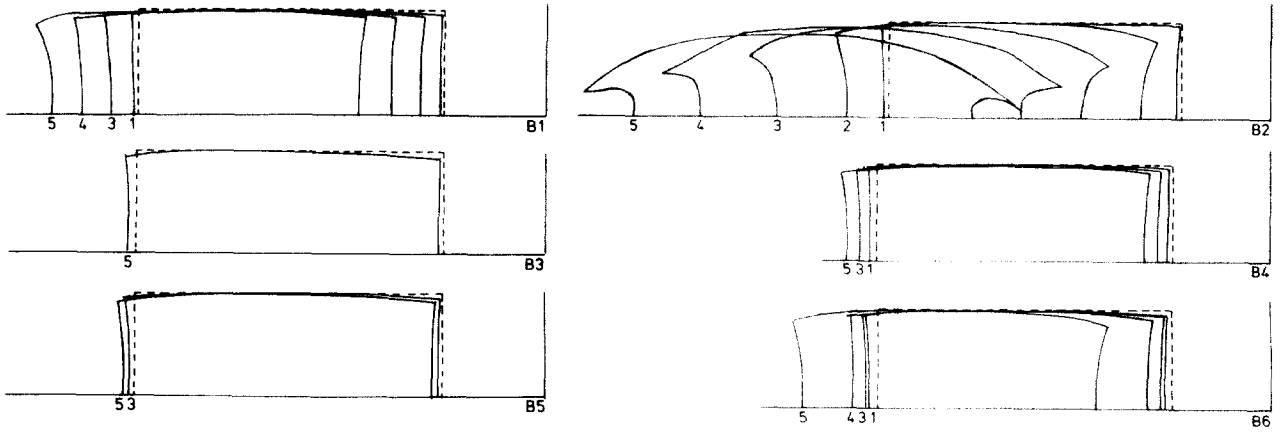

Fig. 4. Variation in boudin shape and separation during progressive (increments 1 to 5) deformation; models B2, B4 and B6 involve boudins which are allowed to yield.

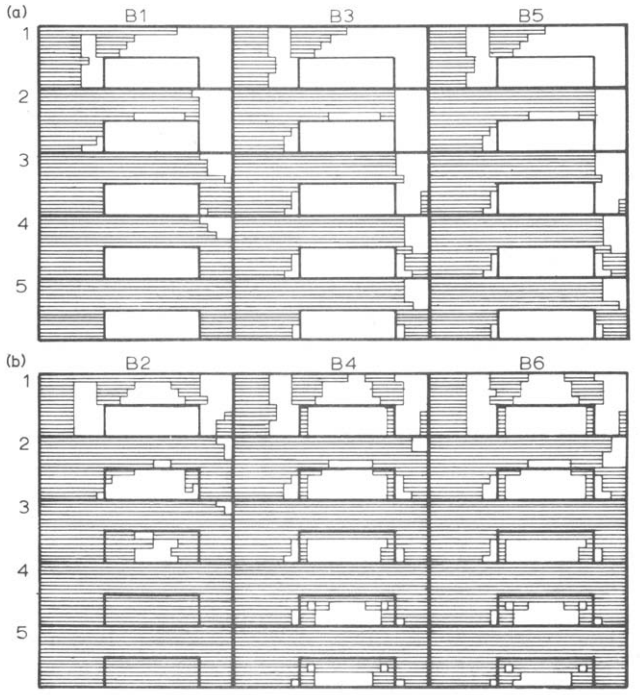

Fig. 5. Variation in equivalent stress in the models as shown by the progressive (increments 1 to 5) development of plastic behaviour (shaded) during deformation. (a) All-elastic boudins. (b) Elastic-plastic boudins.

of deformation the latter two are softer. In each case the matrix yield stress is less than that for the boudin.

The design of the models is shown in Fig. 3; eight node isoparametric elements are used throughout. Because of problems in the formation of new elements during the analysis it was not possible to model the first stages of boudinage, that is the initiation and development of a fracture and the first increments of boudin separation. The models described here take as their starting configuration two boudins which have already separated slightly. Such a geometry has two orthogonal planes of symmetry and we therefore need to model only one quarter of the overall system (Fig. 3). However, this means that the boudin has only a small region of matrix on one (right) side and an infinite extent on the other (left) side. This asymmetry is somewhat unrealistic and leads to slightly asymmetric stress and strain distributions.

The boudinage layer is assumed to be continuous normal to the analysis plane and hence the type of analysis is engineering plane strain. The symmetry axes of each model are constrained so that the nodes can only move parallel to their particular axis. In all models the loads applied at the nodal points along the upper edge are such as to simulate a uniform loading remote from the boudin. This has the same effect on the resulting stresses as removing the component due to the hydrostatic part of the total stress system. The stresses left in the model are therefore due to the stresses which exceed the hydrostatic component.

RESULTS

The results of the PFEM simulations of boudinage are shown in Figs. 4–6. The features of interest are boudin separation, boudin shape and the distribution of stresses within and adjacent to boudins.

Separation

For elastic boudins (models B1, B3, B5) separation increases with decreasing matrix hardness and also with the amount of deformation (Fig. 4). Boudin separation is therefore determined by matrix hardness and amount of deformation. This also applies to models involving plastic boudins; compare B2 (softest) with B4 (hardest). It is interesting to note the separation shown in models B4 and B6. For most of the deformations the stress–strain curves are identical (Fig. 2c) but for the later stages the matrix in model B6 is softer, which allows the boudin to separate more than in B4 (Fig. 4). Close examination of the comparative matrix behaviour for elastic boudins (models B3 and B5) shows a slightly larger separation for the (eventually) softer matrix (B5).

Shape

Because elastic deformation is totally recoverable the three elastic boudins cannot show any permanent shape change. It should be noted that the gross change in shape shown by B1 in Fig. 4 is almost wholly a function of the PFEM. The analytical technique is unable to accommodate the large changes in material behaviour which occur across the boudin–matrix boundary and hence the boudin deforms more than permitted by its elastic moduli in order to maintain element compatibility. In the models involving plastic boudins the initial changes in shape occur at the boudin corners, with the greatest modification being shown by the softest boudin. This is shown especially clearly by comparing models B4 and B6 which have the same boudin stress–strain curves until the later stages of the deformation (Fig. 2b). The shapes are identical until the difference in behaviour occurs when the boudin which is now softer (B6) begins to show more shape modification (Fig. 4). In general, as the deformation continues (increments 1 to 5) the corners continue to deform and the deformation spreads through the boudin. This is best shown by diagrams of the spread of plastic behaviour through the boudins (Fig. 5). Because plastic deformation spreads gradually through the boudin and because the rate of spread is ultimately determined by the hardness of the boudin, hard boudins will show mainly end and corner shape modification but little change in length. Only the softer boudins will extend appreciably (Fig. 4). Boudin shape is therefore determined by boudin hardness and the amount of deformation.

Stress variation

A qualitative appreciation of the stress distribution during boudinage can be gained by tracing the pro-

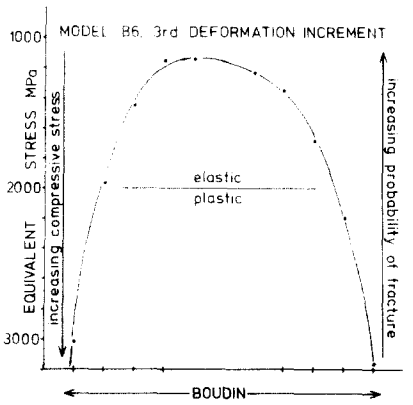

Fig. 6. Variation in equivalent stress along the boudin axis for model B6, third increment.

gressive development of plastic deformation in the models (Fig. 5). Within those boudins that are allowed to yield the stresses are greatest at the ends, especially the corners, as yield occurs there first. As the deformation progresses plastic behaviour gradually develops throughout the boudins, although there is always a central region of relatively lower stress. Models B4 and B6 also show small areas near the corners in which the stress is relatively low. These low stress areas may be anomalies introduced by the PFEM method, but as elastic simulations show similar areas, this seems unlikely. We are unable to offer a physical explanation for these areas.

All the models show the development of matrix pressure shadow regions adjacent to the ends of the boudins (Fig. 5). Pressure shadow regions develop preferentially in hard matrix systems although boudin hardness is a contributing factor.

Figure 6 illustrates the variation in equivalent stress for model B6, load increment 3. The equivalent stress decreases from either end of the boudin implying a trend towards a less compressive stress environment. A consequence of this is that, for any given fluid pressure, the effective stress will be least across the centre of the boudin and therefore tensile fracture is most likely to occur there. Similar fracture behaviour is shown by fibres in fibre-reinforced composites (Kelly 1973) and will be discussed in more detail in the context of boudinage in a subsequent paper.

Summary of results

The results of the PFEM analyses may be summarised as follows.

(1) Boudin separation is a function of matrix hardness and amount of deformation.
(2) Boudin shape is determined by boudin hardness and amount of deformation.
(3) Boudin length can be nearly constant after fracture and during separation but will increase if the boudin is soft.
(4) The largest stresses occur at the ends of boudins, especially the corners, which therefore show the most modification in shape during deformation.

COMPARISON WITH NATURAL EXAMPLES

Boudinage has usually been explained in terms of competence contrast between layer and matrix (e.g. Ramberg 1955, Ramsay 1967, Stromgard 1973, Smith 1975). In what follows we have not used this ambiguous term, instead we use the terms soft and hard to describe in a general way how closely the plastic deformations approach perfect plasticity.

Boudin style

Some common boudinage styles have obviously involved a certain amount of pre-fracture plastic deformation in the form of necking. This is most clearly demonstrated by the pinch-and-swell style of boudinage. Because of the inability of the PFEM to incorporate fracture it has not been possible to consider the effects of pre-fracture plastic deformation and direct comparisons between the simulations and natural boudinage are therefore restricted to situations in which fracture has occurred without prior necking. This appears to be true for the rectangular and barrel styles (Figs. 7a and b). Once fracture has occurred hard boudins will remain approximately rectangular. As hardness decreases the amount of shape modification increases, especially at the corners, resulting in barrel-shaped boudins. With decreasing hardness or increasing deformation the boudin corners may be stretched out into horn-like protuberances (Fig. 7c).

Although not directly applicable, the results of the PFEM analyses can still be used in the interpretation of boudinage which has involved pre-fracture necking. For instance, we can recognise horn-like boudin ends in layers that have suffered considerable pre-fracture necking, thus showing that the post-fracture behaviour was essentially similar to that observed in barrel-shaped boudins. Consequently boudins which have suffered both pre- and post-fracture plastic deformation will show characteristics of both barrel and pinch-and-swell styles (e.g. Cloos 1947, figs. 18 and 19, Ramsay 1967, fig. 3–44).

Very hard boudins suffer no plastic extension either before or after fracture and so, of all the styles of boudinage, only those with nearly rectangular outlines are likely to maintain a constant length during subsequent deformation. All other styles will extend. There may of course be a reduction in boudin length if further fracture occurs. We have not considered fracture in our analyses but the existence of two or more periods of fracturing may be shown by the occurrence of more than one size of inter-boudin gap (e.g. Fig. 7a).

INFILLING OF INTER-BOUDIN GAPS

In our simulations we have taken as a starting con-

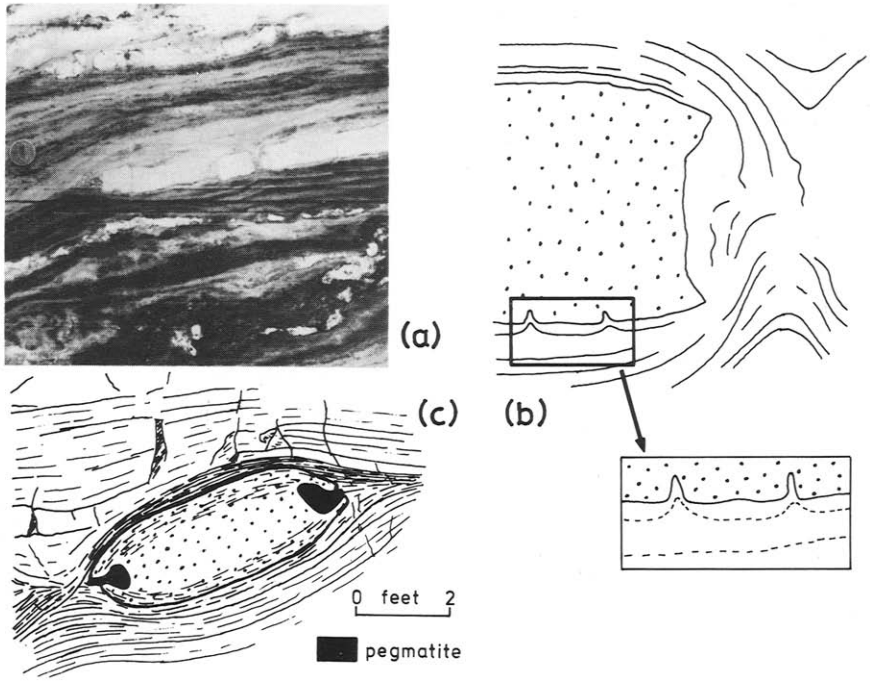

Fig. 7. Styles of boudinage structure considered directly by the PFEM simulations. (a) Rectangular boudins; tremolite layer in marble, Streamstown Marble Quarry, Connemara, Western Ireland. (b) Barrel-shaped boudins; calc-silicate layer in marble (drawn from Ramsay 1967, fig. 3–43). (c) Extreme barrel-shaped boudins; amphibolite sill in quartzite (drawn from Jones 1959, plate XIIA).

figuration two boudins that have already slightly separated. We have therefore assumed the development of a perpendicular fracture through the layer followed by separation, the inter-boudin gap being filled by matrix. In this section we discuss some problems associated with the development and infilling of inter-boudin gaps, our comments being based mainly on observations of natural boudinage.

Inter-boudin gaps filled by minerals crystallised from solution

We assume that the layer normal fractures defining many natural boudins are tension fractures and that effective tensile stresses at depth in the Earth's crust are only possible when the fluid pressure exceeds the confining pressure plus the local tensile strength of the rock at the site of a suitable flaw. There seems little doubt that many inter-boudin gaps are filled by minerals (commonly quartz or calcite) crystallised from the aqueous fluid contained in the resulting crack. In view of the low solubility of, say, quartz in water ($< 1\%$ at 550°C, 4kb and $\sim 0.1\%$ at 300°C, 1 kb, Weil & Fyfe 1964) hundreds or thousands of crack volumes of water would need to be transported through the crack in order for it to be filled. Such a process suggests the existence of an external water reservoir. A more likely alternative is that the crack-filling material is derived by local stress-induced chemical solution and transfer which continually replenishes the crack-filling fluid with ions of the crystalline phase.

The simple model of through-layer fractures followed by gradual boudin separation is expected to result in microstructural features in the inter-boudin gap similar to the vein textures described by Durney & Ramsay (1973). Detailed work may well show many such veins to be the product of repeated crack-seal increments (Ramsay 1980) but many complicating factors can be envisaged. For instance, the boudin-defining fractures may themselves require many small increments of crack extension before eventually forming a through-layer fracture. Indeed, this is to be expected in hydraulic fracturing because, as a sharp flaw develops into a crack, the almost instantaneous increase in volume would lead to sudden loss of fluid pressure. This, combined perhaps with plastic-blunting of the crack-tip, would arrest crack propagation. The vein texture which finally develops depends on whether the short crack seals at this stage or whether fluid pressure rises rapidly again to initiate another propagation event. Once a complete fracture with vein-type infill has developed its subsequent opening history might depend on the stress distribution within the inter-boudin gaps. Each crack-seal event is expected to be concentrated near boudin ends. Early crack-seal increments can therefore eventually become remote from boudin ends and may then suffer subsequent deformation and/or recrystallisation and grain-growth. This may explain inter-boudin gaps showing fibre textures close to boudin ends while further away the grains become more equant.

It should also be remembered that, even in low-grade environments, complex minerals may develop in 'pressure fringes', including tremolite (Wickham 1973) and sericite/white mica (Williams 1972, Mukhopadhyay 1973). At higher grades it may even be possible for pressure fringe mineralogies to be essentially similar to those found in the normal matrix (Ferguson & Harte 1975).

Inter-boudin gaps filled by matrix

Inter-boudin gaps filled by inflow from the surrounding matrix appear to be very common. This type of infill is, of course, expected when boudin separation is preceded by substantial ductile necking, but when found in conjunction with angular boudins it poses some mechanical difficulties. Such infills seem to require, in the early stages of boudin separation, a process analogous to sheet extrusion in order to force matrix into a narrow gap. The high strain-rates necessary would be expected to produce substantial modifications of the matrix microstructure and yet the grain-size and character of foliation found in such inter-boudin gaps is commonly indistinguishable from that in normal matrix remote from the boudinaged layer.

A possible solution to this problem is suggested by the common but puzzling occurrence of angular boudins with wedge-shaped ends or adjacent boudins with otherwise non-matching ends (Fig. 8). These observations suggest that, in spite of their angular appearance, the boudins are not defined by tensile brittle fracture surfaces. Before considering alternative fracture mechanisms we review in the following paragraphs some relevant work on fracture mechanics.

Fracture starts from a pre-existing crack or sharp flaw and it is the conditions in a small volume of material at the crack-tip that determine the subsequent fracture behaviour. The material discontinuity means that no stress can be transmitted across the faces of the crack so that the load which would have been carried by the cracked region is transferred to the surrounding material and is concentrated into a small region near the tip of the crack. For example, if a penny-shaped internal crack of length $2a$ along the x direction lies at right angles to a remote uniaxial tensile stress field, the local stress across the crack plane ahead of the crack is given by,

$$\sigma = K(2\pi x)^{1/2}$$

where K is called the stress intensity factor and, for a fracture stress σ_f, has a critical value of,

$$K_c = \sigma_f(\pi a)^{1/2}.$$

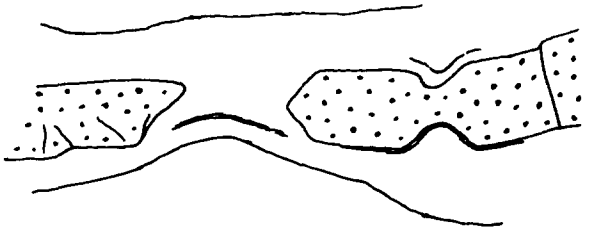

Fig. 8. Example of boudins with non-matching ends, dolomite layer in marble (drawn from Weiss 1972, plate 142A).

K_c is a material property known as fracture toughness which characterises resistance to crack growth.

The situation is more complicated for elastic–plastic materials and much effort has been directed towards finding an analogous one-parameter toughness measure that reflects the elastic–plastic stress and strain fields near the crack-tip. One approach is based on the observation that, when an elastic–plastic body with a sharp crack is subjected to crack-normal uniaxial tension, the crack faces move apart and the crack-tip becomes blunted (without extension of the crack) until some mechanism of crack extension either gradually of abruptly takes over. The critical crack opening displacement, δ_c, is sometimes used as a measure of toughness in yielding fracture mechanics and, for limited plasticity, can be related to K_c through the relation,

$$\delta_c = K_c^2(\sigma_y E)^{1/2}$$

where σ_y is the uniaxial yield stress and E is Young's modulus. The physical significance of δ_c is somewhat problematic because cracks are propagated by release of elastic energy, not by the accumulation of plastic work.

Another one-parameter characterisation is the J-contour integral (see McMeeking 1977), or energy-momentum tensor, which defines for a non-linear elastic deformation the total potential energy release rate (as a crack is extended) for any chosen contour around the crack-tip region. Again J can be related to crack-opening displacement (Turner 1978) but use of a critical J value, J_c, to characterise elastic–plastic fracture again seems difficult to justify because the energy release from a plastic region is quite unlike that from a non-linear elastic region at the same strain level (Knott 1978).

The foregoing remarks are intended to draw attention to the difficulties and uncertainties associated with elastic-plastic fracture mechanics even in relatively straightforward engineering contexts that are amenable to physical experimentation. We will nevertheless attempt to adapt some results of a recent elastic–plastic finite element analysis of crack-tip blunting (McMeeking 1977; see also Rice *et al.* 1979) to the problem of angular boudinage with matrix infill.

The McMeeking study is an incremental finite element analysis which, like ours, uses plane strain isoparametric quadrilateral elements. It is concerned with plastic blunting of a notch rather than a sharp crack. This approach is justified by the earlier work of Rice & Johnson (see McMeeking 1977) who found that the notch shape (calculated by a slip-line method) following small-scale yielding could equally well be obtained from the steady-state shape of an initially sharp crack blunted by the same loads. That is, as the total notch-width grows to several times the original width, the difference between the blunted notch-shape and the shape of a sharp crack blunted by the same loads becomes negligible.

McMeeking's notch-blunting solution for small-scale yielding employs traction-free boundary conditions on the notch surface, and displacement boundary conditions elsewhere. The incremental analysis was continued until final notch-width was about five times the original width, the notch shape remaining unchanged beyond the point at which notch width was about three times the original. There were slight differences in notch-shape depending on whether the material was hardening or non-hardening, that for hardening materials showing a slightly splayed notch (Fig. 9a).

In the context of boudinage the existence of a blunted notch in a layer, rather than a sharp crack, seems important in that it would allow a ductile matrix to infill the notch without posing mechanical difficulties. The blunted notch will still be mechanically weak especially as, in nature, the notch surface is unlikely to be smooth. But such an infilled notch is unlikely to propagate rapidly because its surface would not be traction-free and would therefore be able to transmit stress that would otherwise be concentrated at notch asperities. A further point is that stress concentration at the notch shoulders may well promote yield at these points and hence the notch would widen further.

We visualise boudin-defining fractures developing by this locally plastic mechanism, the final shape of the separation surface depending on the detailed history of crack propagation and crack blunting episodes. In nature, the plastic zone in the crack-tip region may well be rather irregular (examples in metals are given by Prince & Martin 1979, and Hall & Hutchinson 1980). Profound micro-structural modifications may also occur in the plastic region around a crack-tip; in a 28 μm grain-size carbon-steel, for example, Davidson *et al.* (1976) found that subgrains of about 5 μm or less are formed within a zone up to 80 μm from the crack-tip. The subgrains may also depend on the chemical environment at the crack-tip (Lankford & Davidson 1976). For our purposes the important point is that, following a reduction in grain size, deformation mechanisms could operate that show a high strain-rate sensitivity to the stress. As a crack slowly advances the zone of grain refinement left in its wake would allow further permanent deformation. The notch might spread open behind the advancing crack thus allowing the matrix to work its way deeper into the layer. Possible histories of crack development are illustrated in Figs. 9(b–d) and suggest that non-matching ends to adjacent boudins could be due to local plasticity even though the bulk of the layer is not yielding. This model, here offered only as a preliminary suggestion, clearly needs much development, but it does appear to offer a plausible explanation for many occurrences of angular boudins with matrix infill. There is also the attraction that it allows a natural gradation through to boudinage styles that are obviously ductile. Some natural boudinage examples showing features that may be the result of ductile crack opening are shown in Fig. 7(b) (inset, early stage) and Fig. 8 (left hand boudin, later stage).

The model outlined above does not offer an explanation for boudinage structure with matrix infill when adjacent boudins are defined by plane layer-normal surfaces (e.g. Fig. 7a). We find it difficult to account for such occurrences but propose that a rapidly propagating through-layer fracture may be filled with fluid at a pressure close to the confining pressure. The fluid remains

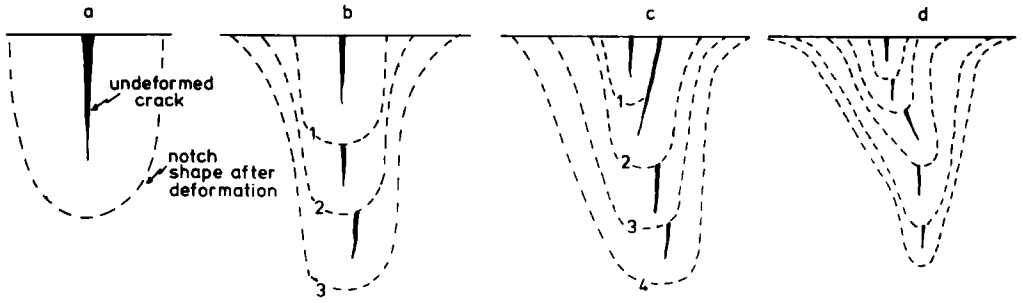

Fig. 9. Diagramatic representation of crack-tip blunting as a possible explanation of boudinage involving boudins with non-matching ends. (a) Development of a blunt notch from a sharp crack in a material with $\nu = 0.3$, $\sigma_0/E = 1/300$, $N = 0.2$ (ν, Poisson's ratio; E, Young's modulus; σ_0, tensile yield strength; N, power-law hardening coefficient), after McMeeking (1977, fig. 2). (b)–(d) Possible development of a notch following successive increments (numbered) of crack advances and crack-blunting; the first crack-blunting increment leads to a notch-shape and, after each increment, matrix is envisaged as filling the notch before the next crack advance.

in the inter-boudin gap during boudin separation, thus providing a hydraulic resistance to the matrix, which does, however, eventually work its way into the gap as separation increases and the fluid gradually escapes. We envisage that such a process would be promoted by pre-fracture dilatancy (Brace *et al.* 1966, Scholz 1968, Edmond & Paterson 1972) such that, following fracture, the fluid held in temporary microcracks would be rapidly drained into the newly developed gap. With the pores thus closed (and permeability consequently reduced) the fluid may then be trapped for a period of time long enough for it to act as a hydraulic 'dashpot' providing resistance against the rapid intrusion of ductile matrix into the inter-boudin gap. The proposed mechanism is illustrated schematically in Fig. 10.

CONCLUSIONS

The term boudinage is used to describe the processes involved in the evolution of structures showing a variety of morphologies which have developed due to the extension and failure of a layer. Consequently in considering boudinage it is important to differentiate between the ductile (plastic) and brittle (fracture) components and also to establish the relationship between them. Plasticity is best considered in terms of the gradient of the stress–strain curve; steep slopes define hard rocks, gentle slopes soft rocks. Fracture may occur at any time during plastic deformation depending on the particular characteristics of the rock. The various combinations of hardness, fracture toughness and timing results in the numerous styles of boudinage, which cannot be adequately explained in terms of competence and competence contrast. The finite element method simulations, although restricted to post-fracture plastic modification, show the importance of boudin hardness in determining boudin shape and matrix hardness in determining boudin separation. The simulations can only be compared directly with natural examples having rectangular or barrel shapes, although the post-fracture behaviour of other styles will be similarly determined by the 'hardness' of boudin and matrix. Early fracturing of hard layers results in rectangular boudins, but for increasingly soft layers barrel and extreme barrel shapes will develop. As the amount of plastic deformation prior to fracture increases necking occurs and cigar or sausage shapes result. The mechanism of fracture also determines the shape of boudins; local plasticity at the site of fracture can lead to the development of boudins with non-matching ends and can also allow the matrix to gradually fill the inter-boudin gaps without losing its essential character.

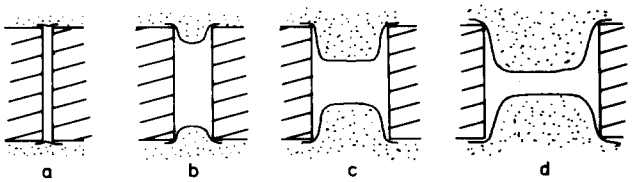

Fig. 10. Schematic representation of progressive (a–d) matrix infill of an inter-boudin gap, the initial boudin separation being a layer-normal plane; ornament indicates boudin (lines), matrix (dots) and fluid (no ornament).

Boudinage is not a simple structural process. To date insufficient consideration has been given to it and many unusual or difficult to explain occurrences have been largely ignored. In this paper we began by considering only the post fracture ductile component of boudin development, but both pre-fracture ductile behaviour and the mechanism of fracture are equally important. Our attempts to relate these various aspects is little more than a faltering start and much more work is required, especially in terms of fracture. There is also the question of chemical changes during boudinage. So far this has been considered only in terms of the infilling of inter-boudin gaps by stress induced solution and transfer. The finite element simulations show that stress gradients exist within boudins and chemical migration might also be expected to occur. In metals, the chemical environment adjacent to fractures or cracks is known to affect the fracture mechanics. The effect of metamorphism during boudinage is also largely unexplored. Misch (1969, 1970) has considered the inter-relationship between deformation and metamorphism but much work needs to be done in this field.

Acknowledgements—We thank Peter Harvey for his comments during the early part of this work and Martin Holder and John Whalley for

reading the manuscript. The finite element analyses were performed with the considerable help of Ray Dawson, Keith Shaw and P.A.F.E.C. Ltd. and were supported by a University of Nottingham postgraduate studentship to G.E.L. The Centre for Materials Science, University of Birmingham (Director, Dr. D. W Jones) provided facilities for manuscript preparation.

REFERENCES

Brace, W. F., Paulding, B. W. & Scholz, C. 1966. Dilatancy in the fracture of crystalline rocks. *J. geophys. Res.* **71,** 3939–3953.

Cloos, E. 1947. Boudinage. *Trans. Am. geophys. Un.* **28,** 626–632.

Davidson, D. L., Lankford, J., Yokobori, T. & Sato, K. 1966. Fatigue crack-tip plastic zones in low carbon steel. *Int. J. Fracture Mech.* **12,** 579–585.

Desai, C. S. & Abel, J. F. 1972. *Introduction to the Finite Element Method.* Van Nostrand Reinhold Company.

Durney, D. W. & Ramsay, J. G. 1973. Incremental strains measured by syntectonic crystal growths. In: *Gravity and Tectonics.* (edited by De Jong, K. A. & Scholten, R.) Wiley, New York, 67–96.

Edmond, J. M. & Patterson, M. S. 1972. Volume changes during the deformation of rocks at high pressures. *Int. J. Rock Mech. & Mining Sci.* **9,** 161–182.

Ferguson, C. C. & Harte, B. 1975. Textural patterns at prophyroblast margins and their use in determining the time relations of deformation and crystallisation. *Geol. Mag.* **112,** 467–480.

Hall, M. G. & Hutchinson, W. B. 1980. Smooth surface metallography using the scanning electron microscope. *Metall. & Mater. Technol.* **12,** 371–375.

Heard, H. C. & Carter, N. L. 1968. Experimentally induced 'natural' intergranular flow in quartz and quartzite. *Am. J. Sci.* **266,** 1–42.

Heard, H. C. & Raleigh, C. B. 1972. Steady-state flow in marbles at 500–800°C. *Bull. geol. Soc. Am.* **83,** 935–956.

Hill, R. 1950. *Mathematical Theory of Plasticity.* Clarendon Press, Oxford.

Huddleston, P. & Stephansson, O. 1973. Layer-shortening and fold shape development in the buckling of single layers. *Tectonophysics* **17,** 299–321.

Jones, A. G. 1959. Vernon map-area, British Columbia. *Geol. Surv. Can. Mem.* **296,** 1–186.

Kelly, A. 1973. *Strong Solids.* Clarendon Press, Oxford.

Knott, J. F. 1978. The fracture toughness of metals. In: *A general Introduction to Fracture Mechanics.* J. Strain Anal. Monog., Mech. Eng. Publ. Ltd., London, 17–31.

Lankford, J. & Davidson, D. L. 1976. Environmental alteration of crack-tip dislocation cell structure and mode of growth during fatigue crack propagation in ferritic steel. *Int. J. Fract.* **12,** 775–776.

McMeeking, R. M. 1977. Finite deformation analysis of crack-tip opening in elastic-plastic material and implications for fracture. *J. Mech. Phys. Solids* **25,** 357–381.

Mendelson, A. 1968. *Plasticity: Theory and Application.* Macmillan, New York.

Mukhopadhyay, D. 1973. Strain measurements from deformed quartz grains in the slaty rocks from Ardennes and the northern Eifel. *Tectonophysics* **16,** 279–296.

Parrish, D. K., Krivz, A. & Carter, N. L. 1976. Finite element folds of symmetry geometry. *Tectonophysics* **32,** 183–207.

Paterson, M. S. 1976. Some current aspects of experimental rock deformation. *Phil. Trans. R. Soc.* **A283,** 163–172.

Prince, K. C. & Martin, J. W. 1979. The effects of dispersoids upon the micromechanisms of crack propagation in Al–Mg–Si alloys. *Acta Metall.* **27,** 1401–1408.

Ramberg, H. 1955. Natural and experimental boudinage and pinch and swell structures. *J. Geol.* **63,** 512–526.

Ramsay, J. G. 1967. *Folding and Fracturing of Rocks.* McGraw-Hill, New York.

Ramsay, J. G. 1980. The crack-seal mechanism of rock deformation. *Nature, Lond.* **284,** 135–139.

Rice, J. R., McMeeking, R. M., Parks, D. M. & Sorenson, E. P. 1979. Recent finite element studies in plasticity and fracture mechanics. *Comput. Methods Appl. Mech. & Eng.* **17/18,** 411–412.

Scholz, C. H. 1968. Microfracturing and the inelastic deformation of rock in compression. *J. geophys. Res.* **73,** 1417–1432.

Selkman, S. 1978. Stress and displacement analysis of boudinage by the finite element method. *Tectonophysics* **44,** 115–139.

Shimamoto, T. & Hara, I. 1976. Geometry and strain distribution of single layer folds. *Tectonophysics* **30,** 1–34.

Smith, R. B. 1975. Unified theory of the onset of folding, boudinage and mullion structure. *Bull. geol. Soc. Am.* **86,** 1601–1609.

Stephansson, O. 1973. The solutions of some problems in structural geology by means of the finite element technique. *Geol. För. Stockh Förh.* **95,** 51–59.

Stephansson, O. & Berner, H. 1971. The finite element technique in tectonic processes. *Phys. Earth & Planet. Interiors* **4,** 301–321.

Stromgard, K. E. 1973. Stress distribution during formation of boudinage and pressure shadows. *Tectonophysics* **16,** 215–228.

Turner, C. E. 1978. Yielding fracture mechanics. In: *A General Introduction to Fracture Mechanics.* J. Strain Anal. Monog., Mech. Eng. Publ. Ltd., London, 32–53.

Weill, D. F. & Fyfe, W. S. 1964. The solubility of quartz in H_2O in the range 1000–4000 bars and 400–500°C. *Geochim. cosmochim. Acta* **28,** 1243–1255.

Weiss, L. E. 1972. *The Minor Structures of Deformed Rocks.* Springer-Verlag, New York.

Wickham, J. S. 1973. An estimate of strain increments in a naturally deformed carbonate rock. *Am. J. Sci.* **273,** 23–47.

Williams, P. F. 1972. 'Pressure shadow' structures in foliated rocks from Bermagui, New South Wales. *J. geol. Soc. Aust.* **18,** 371–377.